Reversal of the Parallel Drift Frequency in Anomalous Transport of Impurity Ions

Shaokang Xu,[1,2] S. Maeyama,[2,3] T.-H. Watanabe[2] and Ö. D. Gürcan[4]

[1]*Southwestern Institute of Physics, P.O. Box 432, Chengdu 610041, People's Republic of China*
[2]*Nagoya University, Furo-cho, Nagoya 464-8602, Japan*
[3]*National Institute for Fusion Science, Toki, Gifu 509-5292, Japan*
[4]*Laboratoire de Physique des Plasmas, CNRS, Ecole Polytechnique, Sorbonne Université, Université Paris-Saclay,
Observatoire de Paris, F-91120 Palaiseau, France*

It is found that, in the studies of heavy ion transport with gyrokinetic simulations, the ion parallel drift frequency can reverse sign in velocity space when the amplitude variation of the electrostatic potential fluctuation is strong along the magnetic field line. As a result, the particle transport related to the parallel dynamics is strongly enhanced. It is noted that, while parallel gradient of the fluctuation amplitude can be instigated by a large magnetic shear or safety factor in a tokamak, the generic mechanism is independent of its cause, which suggests broader applications to kinetic plasma problems. Some relevant topics are briefly addressed in the end.

Introduction.—Turbulence in space and laboratory plasmas has extensively been studied in the past by focusing on phenomena that are perpendicular to the magnetic field lines, as in the case of ion temperature gradient (ITG) driven or trapped electron mode (TEM) turbulence [1–7]. In these cases, the turbulent dynamics parallel to the magnetic field lines are either averaged out as is commonly done for data analysis or resolved using an approximate method as in most analytical calculations [8–13]. For example, in many theoretical studies of plasma turbulence, it is conventional to replace the parallel advection $v_\parallel \nabla_\parallel$ by $ik_\parallel v_\parallel$, with $k_\parallel$, a parallel wave number. This insinuates that the particles with positive and negative parallel velocities along the magnetic field lines also have opposite parallel frequencies, and since the particle transport related to the parallel dynamics is proportional to this parallel frequency, the flux from $v_\parallel > 0$ is canceled or at least significantly reduced by the flux from $v_\parallel < 0$.

In this Letter, we study heavy ion transport with gyrokinetic simulations using the GKV code [14]. We find that the conventional solution with the Fourier transform is actually the contribution of the phase angle of the electrostatic fluctuation to the plasma parallel frequency, and works when the amplitude of the fluctuation has a weak gradient along the magnetic field line. However, when the parallel gradient of the amplitude is enhanced, for example using a large magnetic shear or safety factor, or some other mechanism, the amplitude of the fluctuation can also influence the plasma parallel frequency, resulting in a fraction of particles in velocity space to reverse the sign of their parallel drift, e.g., particles with positive and negative parallel velocities may have parallel frequencies of the same sign, which differs from the conventional

picture. As a result, the particle transport related to the parallel dynamics is strongly enhanced. This is significant as it may change our understanding of the parallel dynamics in the edge of a fusion reactor where the magnetic shear and the safety factor are large, or in a reversed shear configuration. Note that the reversal of the ion parallel drift frequency in plasma turbulence is reported for the first time.

Model.—We study plasma turbulent transport in the gyrokinetic framework. The electrostatic gyrokinetic Vlasov equation is written as [15,16]:

$$\frac{\partial g_s}{\partial t} + v_\parallel \nabla_\parallel g_s + \boldsymbol{v}_{sd} \cdot \nabla g_s + \boldsymbol{v}_{sE} \cdot \nabla g_s$$
$$= \frac{e_s F_{s,M}}{T_s} \frac{\partial \langle \phi \rangle_s}{\partial t} + \boldsymbol{v}_{s*} \cdot \nabla \langle \phi \rangle_s \frac{e_s F_{s,M}}{T_s}, \quad (1)$$

where g_s and ϕ are, respectively, the nonadiabatic part of the perturbed gyrocenter distribution function and the perturbed electrostatic potential. e_s, T_s, and $F_{s,M}$ are the charge, the temperature, and the local Maxwellian equilibrium distribution function of the species s, and $\langle \cdot \rangle_s$ means the gyrophase average, introducing the Bessel function J_{0s} in Fourier space. $v_\parallel$ is the velocity parallel to the magnetic field line, v_{sd}, $\boldsymbol{v}_{sE}$, and $\boldsymbol{v}_{s*}$ denote the magnetic drift velocity, the $E \times B$ drift velocity, and the diamagnetic drift velocity, respectively. From Eq. (1), we find the particle flux related to the perpendicular and the parallel compressibility pinch as follows [17]:

$$\Gamma_s = \frac{k_y |\phi_{k_\perp}|^2}{T_s B_0} \int \frac{J_{0s}^2 e_s F_{sM} (\gamma \omega_{sd} + \gamma \kappa_r v_\parallel - \omega_r \kappa_i v_\parallel) d^3 v}{(\omega_r - \kappa_r v_\parallel - \omega_{sd})^2 + (\gamma - \kappa_i v_\parallel)^2},$$

$$(2)$$

where ω_r is the frequency and γ is the growth rate of the electrostatic potential fluctuation. $\omega_{sd}(\equiv \mathbf{k}_\perp \cdot \mathbf{v}_{sd})$ is the magnetic drift frequency. The first term in the numerator denotes the particle pinch (noted as $\Gamma_{s,\perp}$) due to perpendicular compression. The second and the third terms represent the particle pinch related to parallel dynamics (denoted by $\Gamma_{s,\parallel}$), where $\Gamma_{s,\parallel}(\kappa_r v_\parallel)$ provides the effective contribution and $\Gamma_{s,\parallel}(\kappa_i v_\parallel)$ causes the anisotropy of the particle flux on the magnetic surface and vanishes after the flux surface average [17]. κ is a parallel advection operator defined as $i\kappa \equiv \nabla_\parallel \ln(g_{sk_\perp})$, with $\kappa = \kappa_r + i\kappa_i$. If $\phi_{k_\perp} = \phi_0 e^{ik_\parallel z}$, $\nabla_\parallel \ln(\phi_{k_\perp})$ gives nothing but $ik_\parallel$. Thus, $\kappa_r v_\parallel$, rather than $k_\parallel v_\parallel$, denotes the parallel drift frequency here.

If the parallel advection $v_\parallel \nabla_\parallel$ is replaced by $ik_\parallel v_\parallel$, with $k_\parallel$, a parallel wave number, it turns out that for a given $k_\parallel$, particles with $v_\parallel$ and $-v_\parallel$ take opposite parallel frequencies and contribute in opposite signs to the flux, resulting in the flux from one sign canceling, or at least significantly reducing the flux from the other. This is roughly what happens in our gyrokinetic simulations with a weak magnetic shear or safety factor. In contrast, however, when the gradient of the mode amplitude $|\phi_{b_\perp}|$ is enhanced along the magnetic field line with a strong magnetic shear or safety factor, this picture does not work, and one needs to consider the contribution from the amplitude variation to the ion parallel frequency.

Simulation results.—Simulations are performed for a toroidal plasma in the standard $\hat{s} - \alpha$ geometry with the following parameters: the electron and deuterium density and temperature gradients $R/L_{n,e} = R/L_{n,D} = 2.5$, $R/L_{T,e} = 8.0$, $R/L_{T,D} = 2.0$, respectively, the temperature $T_e = 3T_D$, the inverse aspect ratio $\epsilon = r/R = 0.105$, the safety factor $q = 1.29$, and a realistic electron to deuterium mass ratio $m_e/m_D = 1/3672$ with $m_D = 2$. Magnetic shear $\hat{s}$ is scanned in the interval $[-1.0, 1.3]$. All these cases result in a background turbulence of TEM. Three different heavy ions: carbon C ($m_s = 12$, $e_s = 6+$), iron Fe $(54, 20+)$, and tungsten W $(184, 40+)$ are included in the simulations with a charge fraction of 10^{-4} [18]. Using the simulation data, $\Gamma_{s,\parallel}$ and $\Gamma_{s,\perp}$ are computed. Figure 1 shows $\langle \Gamma_{s,\parallel} \rangle / |\langle \Gamma_{s,\perp} \rangle|$ as a function of the magnetic shear $\hat{s}$, where $\langle f \rangle$ denotes the flux surface average of f defined as $\langle f \rangle = \int \sqrt{g} f \, dz / \int \sqrt{g} \, dz$, with z being the magnetic field line coordinate and $\sqrt{g}$ the Jacobian.

With a weak magnetic shear, i.e., $-0.1 \leq \hat{s} \leq 0.5$, $\Gamma_{s,\parallel}$ is weak in comparison to $\Gamma_{s,\perp}$, and the difference in the particle flux of different ions is due to their charge to mass ratio. Therefore, we also show the normalized $\Gamma_{s,\parallel}$ fluxes [multiplied by $(m_s/m_D)/e_s$] in order to eliminate the e_s/m_s dependence [9,10,17] with the dashed curves. $\Gamma_{s,\parallel}$ and $\Gamma_{s,\perp}$ along the magnetic field line are very similar for carbon and tungsten after normalization, as shown in the subplot (a) of Fig. 1 with $\hat{s} = 0.3$.
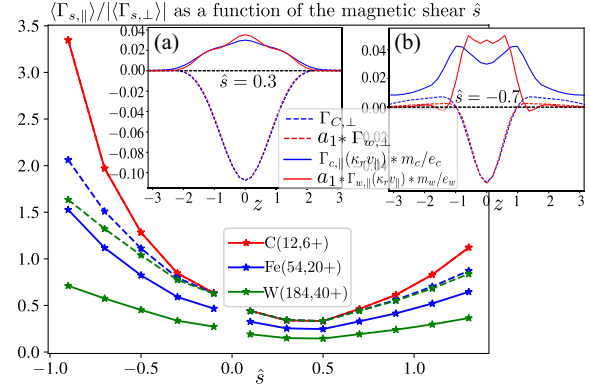
FIG. 1. $\langle \Gamma_{s,\parallel} \rangle / |\langle \Gamma_{s,\perp} \rangle|$ (solid) as a function of the magnetic shear $\hat{s}$ for carbon (red), iron (blue), and tungsten (green). Dashed curves are the normalized flux in $\Gamma_{s,\parallel}$ data multiplied by $(m_s/m_D)/e_s$. The subplots show $\Gamma_{s,\parallel}$ (dashed) and $\Gamma_{s,\perp}$ (solid) of carbon (blue) and tungsten (red) as a function of z, with (a) $\hat{s} = 0.3$ and (b) $\hat{s} = -0.7$. Results are shown for the $k_y \rho_D = 0.3$ mode.

However, with a strong magnetic shear, i.e., $\hat{s} > 0.5$ or $\hat{s} < -0.1$, $\Gamma_{s,\parallel}$ is strongly enhanced in the transport of carbon and iron. For tungsten, $\Gamma_{s,\parallel}$ increases slowly with $\hat{s}$, but with a clear tendency. In this case, the difference in $\Gamma_{s,\parallel}$ of different ions are not simply caused by the e_s/m_s dependence, since the dashed curves in Fig. 1 are different from each other, especially with very strong $\hat{s}$. In particular, with $\hat{s} = -0.9$, the normalized flux of carbon is more than twice that of tungsten. There is certainly a different mechanism that drives this strong transport. $\Gamma_{s,\parallel}$ and $\Gamma_{s,\perp}$ of carbon and tungsten in the simulation with $\hat{s} = -0.7$ are compared in the subplot (b) of Fig. 1. It shows that $\Gamma_{s,\parallel}$ of carbon ions is strongly enhanced in high z regions, compared to that of tungsten.

From Eq. (2), $\Gamma_{s,\parallel}$ is proportional to the parallel advection operator κ, which actually represents the gradient ($\nabla_\parallel$) of the turbulent fluctuation along the magnetic field line. Qualitatively, one may expect that a large parallel gradient of the fluctuation results in a strong parallel compressibility pinch. The profile of the squared electrostatic potential $|\phi_{k_\perp}|^2$ along the magnetic field line in Fig. 2(a) shows that the gradient of the normalized mode amplitude changes with magnetic shear. There is a clear correlation between $\Gamma_{s,\parallel}$ and the parallel gradient of the mode amplitude.

On the other hand, $\Gamma_{s,\perp}$ reverses sign along the field line due to magnetic shear, as $\Gamma_{s,\perp} \propto \mathbf{v}_{sd}$, which reverses sign. In ballooning turbulence like ITG and TEM modes, the fluctuations are very strong on the low field side, where $\Gamma_{s,\perp}$ is directed inward and dominant. Hence, $\Gamma_{s,\perp}$ is usually directed inward in both ITG and TEM turbulence [9,10,17]. A previous fluid simulation reports $\Gamma_{s,\perp}$ changing from inward to outward with a negative magnetic shear
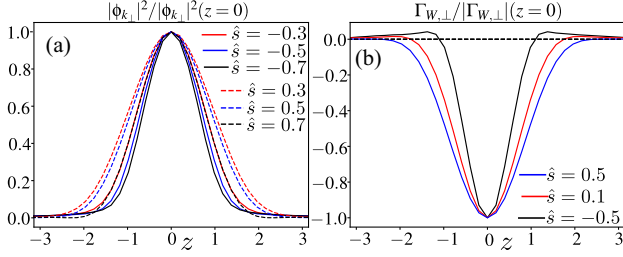
FIG. 2. $|\phi_{\mathbf{k}_\perp}|^2/|\phi_{\mathbf{k}_\perp}|^2(z=0)$ and $\Gamma_{W,\perp}/|\Gamma_{W,\perp}|(z=0)$ as a function of z with different $\hat{s}$. $z=0$ corresponds to the outer middle plane in a tokamak configuration.

by assuming $\omega_r \gg \omega_{sd} \gg k_\parallel v_\parallel$ [11], however, this is not observed in present gyrokinetic simulations with the strong ballooning mode structure. Moreover, the assumption of the turbulence frequencies is also quite different from what we observe. By decreasing $\hat{s}$, the inward transport region of $\Gamma_{s,\perp}$ is decreased, as shown in Fig. 2(b). As a result, when $\hat{s} > 0$, both the normalized $\Gamma_{s,\parallel}$ and $\Gamma_{s,\perp}$ are enhanced with increasing $\hat{s}$, so $\langle\Gamma_{s,\parallel}\rangle$ increases slightly with respect to $\langle\Gamma_{s,\perp}\rangle$. While for $\hat{s} < 0$, $\Gamma_{s,\parallel}$ is enhanced and $\Gamma_{s,\perp}$ is reduced with decreasing $\hat{s}$, resulting in $\langle\Gamma_{s,\parallel}\rangle$ being strongly enhanced with respect to $\langle\Gamma_{s,\perp}\rangle$. Because of the combination of these separate effects of $\hat{s}$ on $\Gamma_{s,\parallel}$ and $\Gamma_{s,\perp}$, we observe the tendency of $\langle\Gamma_{s,\parallel}\rangle/|\langle\Gamma_{s,\perp}\rangle|$ as a function of $\hat{s}$ shown in Fig. 1. The key question is why $\Gamma_{s,\parallel}$ is enhanced when the parallel gradient of the mode amplitude $|\phi_{\mathbf{k}_\perp}|$ becomes large.

Parallel frequency reversal.—Based on Eq. (2), $\Gamma_{s,\parallel}$ is proportional to the parallel frequency $\kappa_r v_\parallel$. Figure 3 shows $\kappa_r v_\parallel$ (top) and $\Gamma_{s,\parallel}(\kappa_r v_\parallel)$ (bottom) of different ions in $(v_\parallel, v_\perp)$ plane in the simulation with $\hat{s} = -0.7$. In the case of tungsten, $\kappa_r v_\parallel$ [Fig. 3(c)] is generally negative (positive)
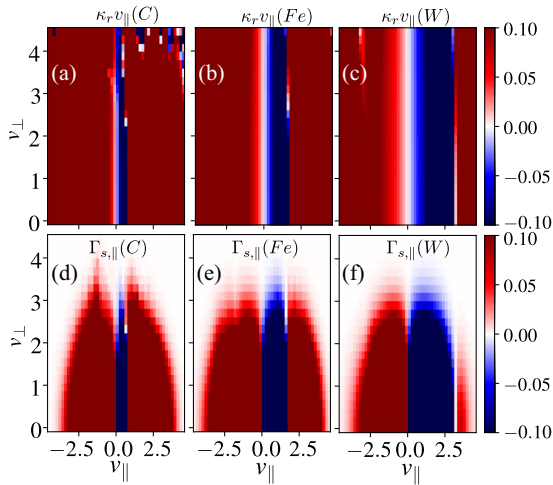
in the positive (negative) $v_\parallel$ zone and symmetric with respect to $v_\parallel = 0$, which is consistent with the conventional solution with $k_\parallel v_\parallel$. Therefore, an outward $\Gamma_{s,\parallel}$ is produced in the negative $v_\parallel$ zone; meanwhile, an inward $\Gamma_{s,\parallel}$ is produced in the positive $v_\parallel$ zone [Fig. 3(f)]. The total $\Gamma_{s,\parallel}$ is small, as $\Gamma_{s,\parallel}(v_\parallel > 0)$ tends to cancel $\Gamma_{s,\parallel}(v_\parallel < 0)$.

We notice that in Fig. 3(c) the parallel frequency of tungsten reverses its sign to positive in the zone of $v_\parallel \geq 3.15$. However, the equilibrium is Maxwellian F_{sM} and $F_{sM}(v_\parallel \geq 3.15) \sim 0$, the frequency reversal in the high $v_\parallel$ zone has little contribution to tungsten flux [Fig. 3(f)]. In the case of iron, $\kappa_r v_\parallel$ follows the conventional description in the low $v_\parallel$ zone of $|v_\parallel| < 1.7$, but reverses sign to positive in the zone of $v_\parallel \geq 1.7$ [Fig. 3(b)], and a non-negligible positive flux is produced [Fig. 3(e)]. In the case of carbon, $\kappa_r v_\parallel$ reverses sign at around $v_\parallel \geq 0.82$ [Fig. 3(a)], and the contribution to the transport flux is significant, since the $\Gamma_{s,\parallel}$, which is directed inward and dominates in the positive $v_\parallel$ zone in the tungsten case, becomes outward in the carbon case, as compared in Figs. 3(d) and 3(f). This qualitative difference strongly enhances the parallel compressibility pinch of carbon ions.

Theoretical analysis.—Here, we explain the parallel frequency reversal by directly resolving the heavy ion parallel frequency. Since $m_s/m_D \gg 1$ and $e_s/e \gg 1$, the gyrokinetic equation of heavy ions is expanded in terms of the zeroth order $\mathcal{L}_0 \sim -i\omega$, the first order $\mathcal{L}_1 \equiv v_\parallel \nabla_\parallel$ and the second order $\mathcal{L}_2 \sim i\mathbf{k}_\perp \cdot \mathbf{v}_{sd}$, [17], with which, we can write: $(\mathcal{L}_0 + \mathcal{L}_1 + \mathcal{L}_2)g_{s\mathbf{k}_\perp} = \mathcal{L}_0(e_s F_{sM} J_{0s}\phi_{\mathbf{k}_\perp}/T_s)$. Expanding $g_{s\mathbf{k}_\perp}$ into $g_{s\mathbf{k}_\perp,0}, g_{s\mathbf{k}_\perp,1}, \ldots$, we find $g_{s\mathbf{k}_\perp,0} = (q_s F_{sM} J_{0s}\phi_{\mathbf{k}_\perp}/T_s)$, $g_{s\mathbf{k}_\perp,1} = -[v_\parallel \nabla_\parallel g_{s\mathbf{k}_\perp,0}/(-i\omega_r + \gamma)]$, and $g_{s\mathbf{k}_\perp,n} = -[(i\omega_{sd}g_{s\mathbf{k}_\perp,n-2} + v_\parallel \nabla_\parallel g_{s\mathbf{k}_\perp,n-1})/(-i\omega_r + \gamma)]$. Here, we solve κ up to the first order with Taylor expansion as follows:

$$i\kappa = \frac{1}{g_{s\mathbf{k}_\perp,0}}\left(\frac{dg_{s\mathbf{k}_\perp,0}}{dz} + \frac{dg_{s\mathbf{k}_\perp,1}}{dz}\right) - \frac{g_{s\mathbf{k}_\perp,1}}{g_{s\mathbf{k}_\perp,0}^2}\frac{dg_{s\mathbf{k}_\perp,0}}{dz} + \cdots. \quad (3)$$

Inserting $g_{s\mathbf{k}_\perp,0}$ and $g_{s\mathbf{k}_\perp,1}$, yielding

$$i\kappa \simeq \nabla_\parallel \ln(J_{0s}\phi_{\mathbf{k}_\perp}) + \nabla_\parallel[v_\parallel \nabla_\parallel \ln(J_{0s}\phi_{\mathbf{k}_\perp})]/i\omega, \quad (4)$$

and the parallel frequency $\kappa_r v_\parallel$ is

$$\kappa_r v_\parallel \simeq v_\parallel \nabla_\parallel \theta_\phi - \frac{\omega_r v_\parallel^2 \nabla_\parallel^2 \ln|\phi_{\mathbf{k}_\perp}|}{\omega_r^2 + \gamma^2}, \quad (5)$$

where $\theta_\phi(\mathbf{k}_\perp, z)$ and $|\phi_{\mathbf{k}_\perp}|(\mathbf{k}_\perp, z)$ are, respectively, the phase and the amplitude of $\phi_{\mathbf{k}_\perp}$ defined as $\phi_{\mathbf{k}_\perp} = |\phi_{\mathbf{k}_\perp}|e^{i\theta_\phi}$. Note that $v_\parallel$ is a function of z in an inhomogeneous magnetic field, and one cannot simply take $v_\parallel$ outside the $\nabla_\parallel$ operator. A term proportional to the mirror force $\mu\nabla_\parallel B$ is neglected

FIG. 3. $\kappa_r v_\parallel$ (top) and $\Gamma_{s,\parallel}(\kappa_r v_\parallel)$ (bottom) in the $(v_\parallel, v_\perp)$ plane for carbon (left), iron (center), and tungsten (right) ions at $z = 1.37$. Results are shown for $k_y\rho_D = 0.3$ with $\hat{s} = -0.7$.
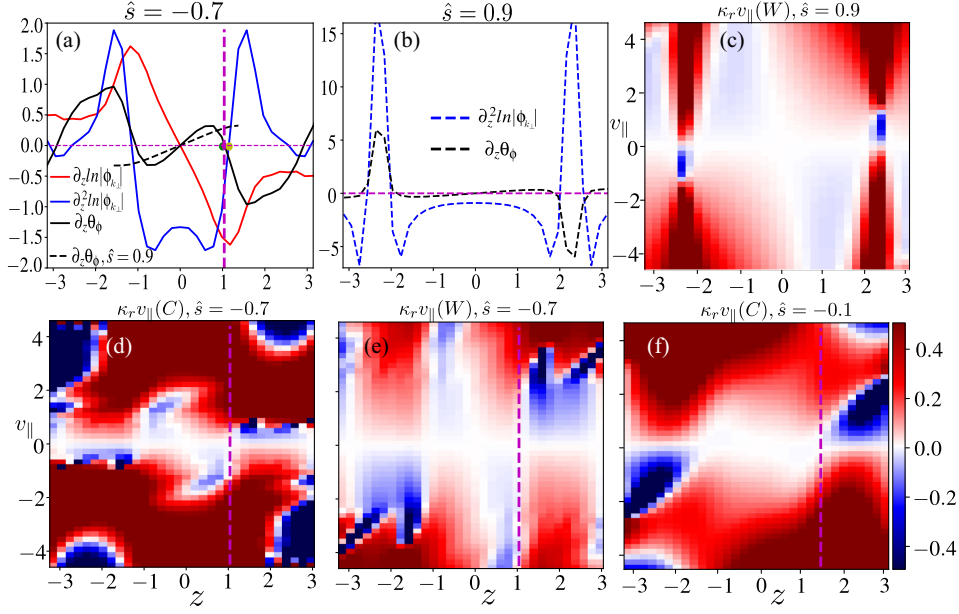
FIG. 4. (a) $\partial_z \theta_\phi$, $\partial_z \ln |\phi_{k_\perp}|$, and $\partial_z^2 \ln |\phi_{k_\perp}|$ as a function of z with $\hat{s} = -0.7$. Black dashed curve shows $\partial_z \theta_\phi$ with $\hat{s} = 0.9$. The green, magenta, and yellow points mark, respectively, the positions where v_{sd}, $\partial_z \theta_\phi$, and $\partial_z^2 \ln |\phi_{k_\perp}|$ are zero. (b) $\partial_z \theta_\phi$ and $\partial_z^2 \ln |\phi_{k_\perp}|$ with $\hat{s} = 0.9$. (c) and (e) show $\kappa_r v_\parallel (v_\parallel, z)$ of tungsten with $\hat{s} = 0.9$ and $\hat{s} = -0.7$. (d) and (f) show $\kappa_r v_\parallel$ of carbon with $\hat{s} = -0.7$ and $\hat{s} = -0.1$. The magenta lines in (a), (d), (e), and (f) mark the position where $\partial_z \theta_\phi = 0$.

in Eq. (5), since $\nabla_\parallel B$ is proportional to the inverse aspect ratio parameter $\epsilon(= 0.105)$, which is small in a large aspect ratio tokamak. Hence, up to the first order, $\kappa_r v_\parallel$ is nearly independent of the perpendicular velocity coordinates, as shown in Fig. 3.

In Eq. (5), the first term is determined by the phase profile of the electrostatic potential, meaning that particles with positive and negative parallel velocity shall have opposite parallel frequency, e.g., the conventional theory may still work. If $\phi_{k_\perp}(z)$ satisfies $\phi_{k_\perp} = |\phi_{k_\perp 0}|e^{ik_\parallel z}$, $\nabla_\parallel \theta_\phi$ gives $k_\parallel$. Hence, the conventional solution with the Fourier transform is actually the contribution of the phase angle θ_ϕ to the plasma parallel frequency in an ideal case: $\theta_\phi(\mathbf{k}_\perp, z) = k_\parallel z$, meanwhile fixing the amplitude $|\phi_{k_\perp}|$ to be constant along the magnetic field line. The second term is determined by the amplitude profile of the electrostatic potential, it is the contribution of the amplitude variation to the plasma parallel frequency, which becomes significant when the gradient of the amplitude is enhanced along the magnetic field line. Moreover, it depends explicitly on the parallel velocity and hence can reverse the sign of the parallel frequency if $v_\parallel$ is large enough. The second term also depends on the frequency ω_r and hence the parallel frequency shall be different under different turbulence regimes. Note that the role of the mode amplitude in the plasma parallel frequency in plasma turbulence is reported for the first time here.

Figure 4(a) shows $\partial_z \theta_\phi$, $\partial_z \ln |\phi_{k_\perp}|$, and $\partial_z^2 \ln |\phi_{k_\perp}|$ along the magnetic field line with $\hat{s} = -0.7$. $\partial_z \theta_\phi$, $\partial_z^2 \ln |\phi_{k_\perp}|$, and

the magnetic drift velocity v_{sd} reverse the sign almost in the same position, as marked by the magenta, yellow, and green circles, respectively. When $\partial_z \theta_\phi$ is close to zero [marked by the magenta lines in Figs. 4(d) and 4(e)], $\kappa_r v_\parallel$ starts to reverse the sign, since the second term plays a role. The frequency reversal occurs in the low velocity zone and exists in a long region in the z direction ($z > 1.0$, $v_\parallel \gtrsim 0.7$) in the carbon case [Fig. 4(d)]. However, with $\hat{s} = -0.1$, the gradient of the mode amplitude is small, the frequency reversal also occurs, but in high velocity zone in Fig. 4(f). The frequency reversal is also observed in the tungsten case with $\hat{s} = -0.7$, but occurs in the high velocity zone and exists only in a narrow region [Fig. 4(e)]. Figure 4(b) shows the profile of $\partial_z \theta_\phi$ and $\partial_z^2 \ln |\phi_{k_\perp}|$ with $\hat{s} = 0.9$. Compared to $\hat{s} = -0.7$, $\partial_z^2 \ln |\phi_{k_\perp}|$ is much larger, but $\partial_z \theta_\phi$ is smaller, e.g., the influence of the mode amplitude is stronger with a large positive magnetic shear. Hence, the parallel frequency
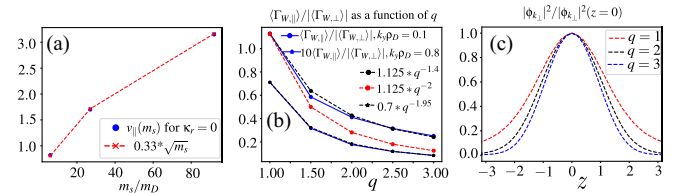
FIG. 5. (a) $v_\parallel(\kappa_r = 0)$ as a function of mass m_s at $z = 1.37$ with $\hat{s} = -0.7$. (b) $\langle \Gamma_{W,\parallel} \rangle / |\langle \Gamma_{W,\perp} \rangle|$ (blue) as a function of q for $k_y \rho_D = 0.1$ and $k_y \rho_D = 0.8$ modes, here $\hat{s} = 0.3$. (c) $|\phi_{k_\perp}|^2 / |\phi_{k_\perp}|^2(z=0)$ as a function of z with different q.

reverses sign in the low velocity zone even in the tungsten case in Fig. 4(c). Finally, $\langle\Gamma_{s,\parallel}\rangle/|\langle\Gamma_{s,\perp}\rangle|$ increases even though $\Gamma_{s,\perp}$ is very strong with a large positive $\hat{s}$. The result in Fig. 1 is shown for the $k_y\rho_D = 0.3$ mode. Actually, $\langle\Gamma_{s,\parallel}\rangle$ is much stronger for the $k_y\rho_D = 0.1$ mode [17], for example, $\langle\Gamma_{W,\parallel}\rangle/|\langle\Gamma_{W,\perp}\rangle|$ is 0.8 with $\hat{s} = 1.3$. Based on this tendency, $\Gamma_{s,\parallel}$ can exceed $\Gamma_{s,\perp}$ with a stronger positive magnetic shear.

As $v_\parallel$ is normalized by the thermal speed $\sqrt{T_s/m_s}$, from Eq. (5) we predict that

$$v_\parallel(\kappa_r = 0) \propto \sqrt{m_s}, \tag{6}$$

e.g., the $v_\parallel$ where the parallel frequency reverses the sign in velocity space follows a $\sqrt{m_s}$ scaling. This is well confirmed by the simulations, as shown in Fig. 5(a). To further confirm the validity of the above results, we fix $\hat{s} = 0.3$, but vary the safety factor q. Based on the lowest order solution, $\langle\Gamma_{W,\parallel}\rangle/|\langle\Gamma_{W,\perp}\rangle|$ follows a $1/q^2$ scaling, as $v_\parallel\nabla_\parallel(v_\parallel\nabla_\parallel) \sim 1/q^2$. However, Fig. 5(c) shows that the parallel gradient of the amplitude $|\phi_{\mathbf{k}_\perp}|$ is enhanced with increasing q in the present case, one may think that $\Gamma_{W,\parallel}$ may be enhanced with a high q. Indeed, $\langle\Gamma_{W,\parallel}\rangle/|\langle\Gamma_{W,\perp}\rangle|$ follows a $1/q^{1.4}$ ($1/q^{1.2}$ for carbon) scaling for the $k_y\rho_D = 0.1$ mode in Fig. 5(b). For high k_y modes with high frequency, the influence of the mode amplitude is mitigated and $\langle\Gamma_{W,\parallel}\rangle/|\langle\Gamma_{W,\perp}\rangle|$ is close to $1/q^2$. From this result, one shall find that various parameters, not only the magnetic shear, can modify the fluctuation profile along the magnetic field line.

Summary.—We report the reversal of the parallel drift frequency when the gradient of the mode amplitude is enhanced along the magnetic field line. As a result, the ion fluxes related to the parallel dynamics are seen to be strongly enhanced, rather than reduced or suppressed.

The heavy ion parallel frequency $\kappa_r v_\parallel$, rather than $k_\parallel v_\parallel$, is derived for the first time in the gyrokinetic framework, which depends on the parallel gradient of the phase angle ($\sim v_\parallel\nabla_\parallel\theta_\phi$) and the second derivative of the mode amplitude ($\sim v_\parallel^2\nabla_\parallel^2\ln|\phi_{\mathbf{k}_\perp}|/\omega_r$). The former gives an opposite frequency for particles with $v_\parallel$ and $-v_\parallel$, and tends to suppress the transport, while the latter gives the same frequency for $v_\parallel$ and $-v_\parallel$ particles and tends to enhance the transport. The ion flux related to parallel dynamics is a competition of these two and codetermined by the ion mass, the turbulence frequency, and the (phase and amplitude) profile of fluctuations. Phase and amplitude separation, which is initially applied to the Vlasov-Poisson system in the study of Landau damping [19,20], is now proved to be a powerful tool to understand many complicated problems [21–25].

We emphasize that the parallel frequency reversal can be triggered by various parameters in plasma turbulence, and not only the magnetic shear and the safety factor shown here. Future research should address other possible mechanisms as well as key fundamental questions on the proper description of parallel drift frequency of ions and electrons in kinetic plasma turbulence, its influence on various transport fluxes, and their dependencies on different turbulence regimes and magnetic configurations.

[1] T. Görler and F. Jenko, Phys. Rev. Lett. **100**, 185002 (2008).
[2] Z. Lin, T. S. Hahm, W. W. Lee, W. M. Tang, and R. B. White, Science **281**, 1835 (1998).
[3] X. Garbet, Y. Idomura, L. Villard, and T. Watanabe, Nucl. Fusion **50**, 043002 (2010).
[4] S. Maeyama, Y. Idomura, T.-H. Watanabe, M. Nakata, M. Yagi, N. Miyato, A. Ishizawa, and M. Nunami, Phys. Rev. Lett. **114**, 255002 (2015).
[5] S. Maeyama, T.-H. Watanabe, M. Nakata, M. Nunami, Y. Asahi, and A. Ishizawa, Nat. Commun. **13**, 3166 (2022).
[6] J. Citrin, C. Bourdelle, P. Cottier, D. F. Escande, Ö. D. Gürcan, D. R. Hatch, G. M. D. Hogeweij, F. Jenko, and M. J. Pueschel, Phys. Plasmas **19**, 062305 (2012).
[7] J. Candy and R. E. Waltz, J. Comput. Phys. **186**, 545 (2003).
[8] X. Garbet, L. Garzotti, P. Mantica, H. Nordman, M. Valovic, H. Weisen, and C. Angioni, Phys. Rev. Lett. **91**, 035001 (2003).
[9] C. Angioni and A. G. Peeters, Phys. Rev. Lett. **96**, 095003 (2006).
[10] C. Bourdelle, X. Garbet, F. Imbeaux, A. Casati, N. Dubuit, R. Guirlet, and T. Parisot, Phys. Plasmas **14**, 112501 (2007).
[11] S. Futatani, X. Garbet, S. Benkadda, and N. Dubuit, Phys. Rev. Lett. **104**, 015003 (2010).
[12] C. Angioni, Plasma Phys. Control. Fusion **63**, 073001 (2021).
[13] T.-H. Watanabe, S. Maeyama, and M. Nakata, Nucl. Fusion **63**, 054001 (2023).
[14] T.-H. Watanabe and H. Sugama, Nucl. Fusion **46**, 24 (2005).
[15] P. H. Rutherford and E. A. Frieman, Phys. Fluids **11**, 569 (1968).
[16] E. A. Frieman and L. Chen, Phys. Fluids **25**, 502 (1982).
[17] S. Xu, S. Maeyama, and T.-H. Watanabe, Phys. Rev. Res. **4**, 043156 (2022).
[18] T. Pütterich, R. Neu, R. Dux, A. Whiteford, M. O'Mullane, and H. Summers (the ASDEX Upgrade Teams), Nucl. Fusion **50**, 025012 (2010).

[19] S. Xu, Z. B. Guo, and O. D. Gürcan, Phys. Rev. E **103**, 023208 (2021).

[20] Z. B. Guo, Y. H. Wang, and S. K. Xu, Phys. Rev. E **101**, 030201(R) (2020).

[21] A. Ghizzo, D. Del Sarto, and H. Betar, Phys. Rev. Lett. **131**, 035101 (2023).

[22] A. Ghizzo and D. D. Sarto, Nucl. Fusion **63**, 104002 (2023).

[23] A. Ghizzo and D. Del Sarto, Phys. Plasmas **29**, 042507 (2022).

[24] O. D. Gürcan, J. Anderson, S. Moradi, A. Biancalani, and P. Morel, Phys. Plasmas **29**, 052306 (2022).

[25] F. Haas, J. T. Mendonça, and H. Terças, Phys. Rev. E **108**, 055203 (2023).